

Mechanisms of Fluorescence Quenching in Prototypical Aggregation-Induced Emission Systems: Excited State Dynamics with TD-DFTB

Received 00th January 20xx,
Accepted 00th January 20xx

DOI: 10.1039/x0xx00000x

www.rsc.org/

Thierry Tran,^a Antonio Prlj,^{a*} Kun-Han Lin,^a Daniel Hollas,^a and Clémence Corminboeuf^{a*}

A recent implementation of time-dependent tight-binding density functional theory is employed in excited state molecular dynamics for the investigation of the fluorescence quenching mechanism in 3 prototypical aggregation-induced emission systems. An assessment of the accuracy of electronic structure method is done by comparison with previous theoretical work while dynamics simulations were extended to condensed phase to obtain excited state lifetimes comparable to experiment. A thorough investigation is done on tetraphenylethylene in order to resolve the on-going debate on the role of specific deactivation mechanisms. Both gas phase and solvent dynamics were computed for fulvene and silole derivatives.

1 Introduction

Small organic fluorescent molecules are a class of compounds with a wide range of applications in fields such as imaging and sensing,^{1–3} optoelectronics,^{4,5} and photodynamic therapy.⁶ Among these small organic molecules, some chromophores have the unusual property of being non-fluorescent in solution and emissive in the solid state/aggregate. This important photophysical phenomenon is called aggregation-induced emission (AIE), first reported in 2001 by Luo *et al.*⁷ for silole derivatives. Since this discovery, the design of AIE-active molecules and their applications have become a topic of high interest.^{8–15}

To design efficient AIE systems, a fundamental understanding of their excited state deactivation pathways is essential. Many experimental and theoretical works have tried to provide a photophysical rationale for the AIE phenomenon. Two major mechanisms have been proposed: the restriction of intramolecular motion (RIM)^{8,16–18} and the restricted access to conical intersection (RACI).^{19–21} Both models try to rationalize the twofold process: i) fluorescence quenching in solution and ii) induced fluorescence in the aggregate. Several other explanations of the induced emission can be found in the literature, such as the formation of excimers²² and J-aggregates,^{23,24} and intramolecular planarization.²⁵ In the general RIM model, the motions such as the vibrations and rotations which are responsible for the nonradiative decay of

excited state in solution (by dissipating energy to the environment) are blocked upon aggregation. The hindered motion induces radiative decay through fluorescence. This model is currently accepted as the state-of-the-art by the experimental community.^{8,9,15,26} In the RACI model, which has gained more importance recently, the molecule in solution can decay to the ground state due to the presence of an energetically accessible conical intersection (*i.e.* crossing seam) between the potential energy surface of the excited state and the ground state. Upon aggregation, the conical intersection is no longer energetically accessible and the molecule relaxes to the ground state radiatively through fluorescence. Both models agree that the restriction of intramolecular motion is responsible for the induced fluorescence in aggregate. However, the main challenge that remains is to unravel the detailed (*i.e.* atomistic) mechanisms behind the fluorescence quenching in solution.

In the earlier work, the main explanation for the fluorescence quenching of the most representative AIE molecules, such as tetraphenylethylene (TPE),^{27–29} diphenyldibenzofulvene (DPDBF),^{30,31} and silole derivatives³² was in terms of energy dissipation through the intramolecular motion upon photoexcitation. However, this explanation (in the spirit of RIM hypothesis) appears somewhat vague and too general. Recent investigations have shown the importance of conical intersection for the deactivation of excited state in these molecules.^{19,20,33,34} Moreover, it was reported that the excited state decay of TPE^{35–37} and DPDBF³¹ in solution occurs at the picosecond timescale. The nonradiative decay on ultrafast timescales is consistent with dynamics involving conical intersections, rather than the vibration-mediated decay (typically described within the Fermi's golden rule approximation) which occurs on the nanosecond to

^a Laboratory for Computational Molecular Design, Institute of Chemical Sciences and Engineering, Ecole polytechnique fédérale de Lausanne (EPFL), CH-1015 Lausanne, Switzerland. E-mail: clemence.corminboeuf@epfl.ch

† Electronic Supplementary Information (ESI) available: Parameters for the nonadiabatic dynamics and additional analysis of the electronic population and mechanic. See DOI: 10.1039/x0xx00000x

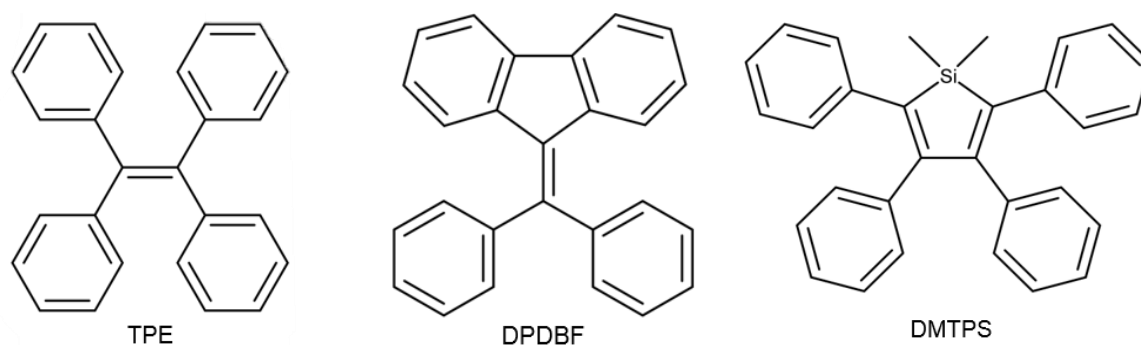


Fig. 1: Investigated molecules: (a) tetraphenylethylene, (b) diphenyldibenzofulvene and (c) dimethyltetraphenylsilole

microsecond timescales.³⁸ The assessment of accessibility of conical intersections and their localization on a potential energy surface are a computational challenge for large systems.

The present work has a twofold objective. Our primary goal is to employ a computational protocol to investigate the fluorescence quenching mechanisms of the relatively large molecular systems in solution. Nonadiabatic dynamics will give insight into the main deactivation pathways as well as the possible side-channels for the nonradiative decay. The computation in the presence of solvent will grant us the possibility to qualitatively determine solvation effect on the timescales and decay mechanisms and to make direct comparison with available experiments. However, reaching such timescales is challenging for the standard quantum chemical methods (such as TD-DFT, wavefunction-based). Thus the second goal is to validate the accuracy of a recently proposed linear-response time-dependent tight-binding density functional theory (TD-DFTB) with long-range correction (LC-TD-DFTB).^{39–41} LC-TD-DFTB is a promising method to describe complex and big system due to its low computational cost. We employ a nonadiabatic molecular dynamics in the framework of LC-TD-DFTB, which was recently implemented by Mitric *et al.*^{41–43} The three prototypical AIE systems (TPE, DPDBF and dimethyltetraphenylsilole, DMTPS; see Fig. 1) investigated in this work are the ideal model systems to confirm the reliability of LC-TD-DFTB due to available computational results obtained at higher levels of theory (TD-DFT, CASPT2).^{19,20,33,34} To find the most appropriate TD-DFTB approximation, we particularly focus on TPE, for which dynamic investigations already exist (gas phase).^{33,34} Thus, the “benchmarking” part (section 3.1.1) refers to the system in the gas phase. Overall, a validation of the reliability of TD-DFTB will offer the possibility to use this new promising method for rational design and screening of new AIEgens with superior properties.

2 Computational details

2.1 Electronic structure methods

The electronic structure was described using LC-TD-DFTB within the monopole approximation, as implemented by Mitric *et al.* in DFTBaby 0.1.0 code.^{41–43} We use the default DFTB parameters in DFTBaby which are based on the *mio*

parametrization; all TD-DFTB computation are done with these parameters unless stated otherwise. The two available implementations of long-range correction^{41,44,45} were used for the three investigated molecules. The main difference between the two long-range corrections is the functional used at DFT level of theory to obtain the reference density. In the original implementation (LC1) by Mitric *et al.*, the DFTB Hamiltonian is based on a local exchange correlation functional with a GGA reference density (*i.e.* PBE) and the long-range contribution is included using the full density. The latter implementation (LC2) by Niehaus *et al.* is based on the Hamiltonian evaluated with BNL functional and the long-range correction is added using a difference of density. It was argued that using a difference of density for the long-range contribution is a more sensible choice rather than using the full density matrix (*i.e.* LC1-TD-DFTB).⁴²

The TD-DFTB, TD-DFT and ADC(2) gas phase vertical excitation energies were computed at the ground state geometry optimized at ω B97XD⁴⁶/Def2-SVP⁴⁷. The geometry optimization and TD-DFT vertical excitation energies were computed with Gaussian 09.⁴⁸ The TD-DFTB (with *mio* parameter) and ADC(2) vertical excitation energies were computed with DFTBaby and Turbomole 7.1,⁴⁹ respectively. The TD-DFTB vertical excitation energies with *3ob* parameter were computed with DFTB+ 18.1.⁵⁰

2.2 QM/MM approach

The computation in solvent was performed using a QM/MM (quantum mechanics/molecular mechanics) approach. We extended the already existing framework for QM/MM in DFTBaby and implemented an interface to Gromacs 5.1.4.^{51,52} The interactions of the atoms in the MM part are described with the General Amber Force Field (GAFF).⁵³ The QM region of the system consists of the AIE molecule and the solvent is made of 100 molecules of hexane. A mechanical embedding is used for the QM/MM computation which is sufficient to describe the interaction of the nonpolar AIE molecule with an apolar solvent such as hexane. Thus, the small polarization of the QM part by the partial charges of the MM part may be ignored.

2.3 Spectra, dynamics and initial conditions

The photoabsorption spectra of both TPE and the cyclized form of TPE (c-TPE) are computed from the vertical excitation

energies (the 2 lowest singlet states) with LC2-TD-DFTB. 500 structures (both TPE and c-TPE) were taken from a semi-classical Wigner distribution based on the ground state harmonic vibrational frequencies. The spectral transitions were broadened by a Lorentzian with a phenomenological broadening of 0.1 eV.

Two types of dynamics (nonadiabatic and adiabatic) were performed based on the interstate gap between S_1 and S_2 (see Table S1 and S3 in ESI for details) for all 3 molecules. The nonadiabatic dynamics within the framework of Tully's fewest switches surface hopping⁵⁴ was computed using a time step of 0.1 fs and the nonadiabatic couplings were computed between three lowest singlet excited states. The adiabatic dynamics (*i.e.* dynamics restricted to the S_1 state) was performed using a time step of 0.5 fs and considering only the ground and S_1 state, in order to speed-up the computation. Simulations were run for all 3 molecules in both gas phase and solution using the two implementations of long-range correction, LC1 (see ESI) and LC2 (see section 3). A comparison is done with standard TD-DFTB (without long-range correction) for TPE with both *mio* and *3ob* parameters for the electronic structure. The adiabatic dynamics is performed using ABIN code⁵⁵ with a time step of 0.48 fs (*i.e.* 20 a.u.) while the electronic structure is computed with DFTB+ 18.1 (DFTB3).⁵⁰ An overview of all the performed dynamics simulations is given in the ESI (Table S3).

The initial conditions (atomic positions and velocities) for the gas phase molecular dynamics were generated using Wigner distribution (with harmonic frequencies from ω B97XD/Def2-SVP). The initial conditions for the molecular dynamics in solvent were prepared following a variation of a protocol suggested by Ruckebauer *et al.*⁵⁶ where the initial conditions of the QM part were generated from a Wigner distribution in gas phase. The unit cell for the system was generated by putting the frozen solute molecule in the center and filling the remaining space with 100 hexane molecules randomly with the density of 0.655 g/cm³ using Packmol.⁵⁷ The generated unit cell undergoes a structure relaxation. The system was then equilibrated at 300 K (with the canonical velocity rescaling thermostat),⁵⁸ with a time coupling constant of 1 ps for 1 ns of dynamics and a time step of 1 fs. In all the steps, the solute was kept frozen. Bonds involving hydrogen atoms were constrained using a linear constraint solver algorithm. The dynamics was performed with Gromacs 5.1.4.

A swarm of 100 trajectories was initiated in the brightest low-lying singlet excited states for all systems except for nonadiabatic dynamics in solution where for some systems a swarm of only 30 trajectories were propagated due to the higher computational cost (*i.e.* longer timescales and slower dynamics, see Table S3 in ESI for details). Each system (isolated and solvated molecules) was propagated within the NVE ensemble. All simulations were performed with DFTBaby code, which was interfaced to Gromacs for dynamics in solution. Trajectories were propagated until the S_1/S_0 crossing was reached (*i.e.* up to a certain gap threshold value; see Table S3 in ESI for details) which is a common practice when single reference methods are employed.^{59,60} We assume that for

trajectories reaching the intersection region, excited state population is transferred to the ground state.

The excited state lifetime is obtained by fitting the excited state population to a single exponential decay function $f(t) = \exp(-(t-t_d)/t_f)$ where t_d is the time delay before the population of ground state start to raise and t_f is the time decay. The lifetime τ is computed by adding time delay and decay (see Table S4 in ESI for overall lifetimes in all dynamics simulations).

3 Results and Discussions

3.1 Excited state dynamics of TPE

The excited state dynamics of TPE has been investigated since the early 70s.^{27–29,33–37,61–68} Yet, the interpretation of the excited state decay is still somewhat controversial. The initial interpretations mainly considered ethylenic twist the main deactivation pathway.^{35,37,61} Other studies pointed out the importance of the torsional motion of the phenyl rings.^{36,62,69} As the field of AIE advanced, since 2001, the torsional motion

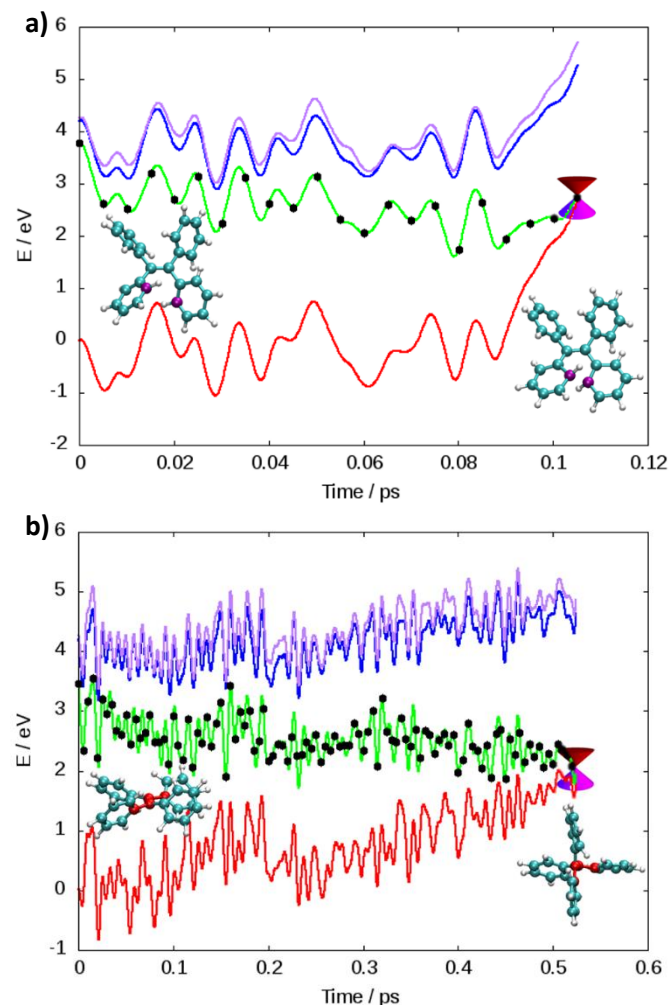


Fig. 2: Energy profile of two illustrative trajectories from dynamics at LC2-TD-DFTB following (a) the photocyclization with the carbon atoms involved in cyclization in purple and (b) the ethylenic twist where a significant change of the CC=CC dihedral angle (carbon atoms in red) can be observed. Potential energies of $S_0/S_1/S_2/S_3$ are shown in red/green/blue/magenta, while all the energies are relative to the initial ground state energy.

was considered the main decay channel in the framework of RIM.^{27,28,62,63,67} Recently, two computational groups (including our own) have shown the importance of photocyclization, which can be rationalized from Woodward-Hoffmann rules.^{33,34} Photocyclization indeed involves some torsional motion of phenyl rings. Occasionally, the proof of cyclization can also be found in experimental literature.^{66,70–74} Still, the most recent work stated that the ethylenic twist plays the crucial role in the fluorescence quenching of TPE.^{64–66}

Although there is still no final consensus about the excited state dynamics of TPE, identifying the TD-DFTB approximation which could qualitatively reproduce DFT results (gas phase) would be extremely useful, as it would allow significant computational speedup. This opens the possibility to investigate longer timescales, which are important for dynamics in condensed phase. On the other hand, dynamics in solvent could be directly compared to available experiments, which will be the additional test for the proposed computational protocol.

3.1.1. Comparison of different TD-DFTB approaches

We initiate the excited state dynamics in the optically bright S_1 state and using nonadiabatic and adiabatic dynamics, a detailed comparison for the deactivation mechanisms of TPE in gas phase is done for the different implementations of TD-DFTB.

Two main deactivation mechanisms of TPE were identified, photocyclization and ethylenic twist (see Fig. 2). The shape of the excited state population decay (see Fig. S4-d in ESI) indicates that two mechanisms have a slightly different timescale. The “fast” deactivation mechanism corresponds to the photocyclization which involves a small torsion of the phenyl rings. The “slow” deactivation mechanism is the ethylenic twist where a more significant geometrical reorganization of the molecule is necessary in order to reach the conical intersection.

The presence of two mechanisms can be outlined by plotting the minimum distance between the carbon atoms involved in the cyclization and the twisting dihedral angle of TPE (see Fig. 3). Two major mechanisms are represented by the two regions of black dots, which correspond to the geometries at S_1/S_0 crossing for the different trajectories. The black dots at 2 Å correspond to the photocyclization and the region with a high dihedral angle (close to 90°) represents the ethylenic twist. The red dots correspond to the nuclear geometries during the dynamics, thus the density of red dots represents the regions of configurational space where molecule spends most of the time. Note that TD-DFT dynamics is based on a smaller number of trajectories and slightly different sampling of initial conditions.³³ For that reason we do not directly compare the population decay (Figure S4). The ratio between two mechanisms critically depends on the

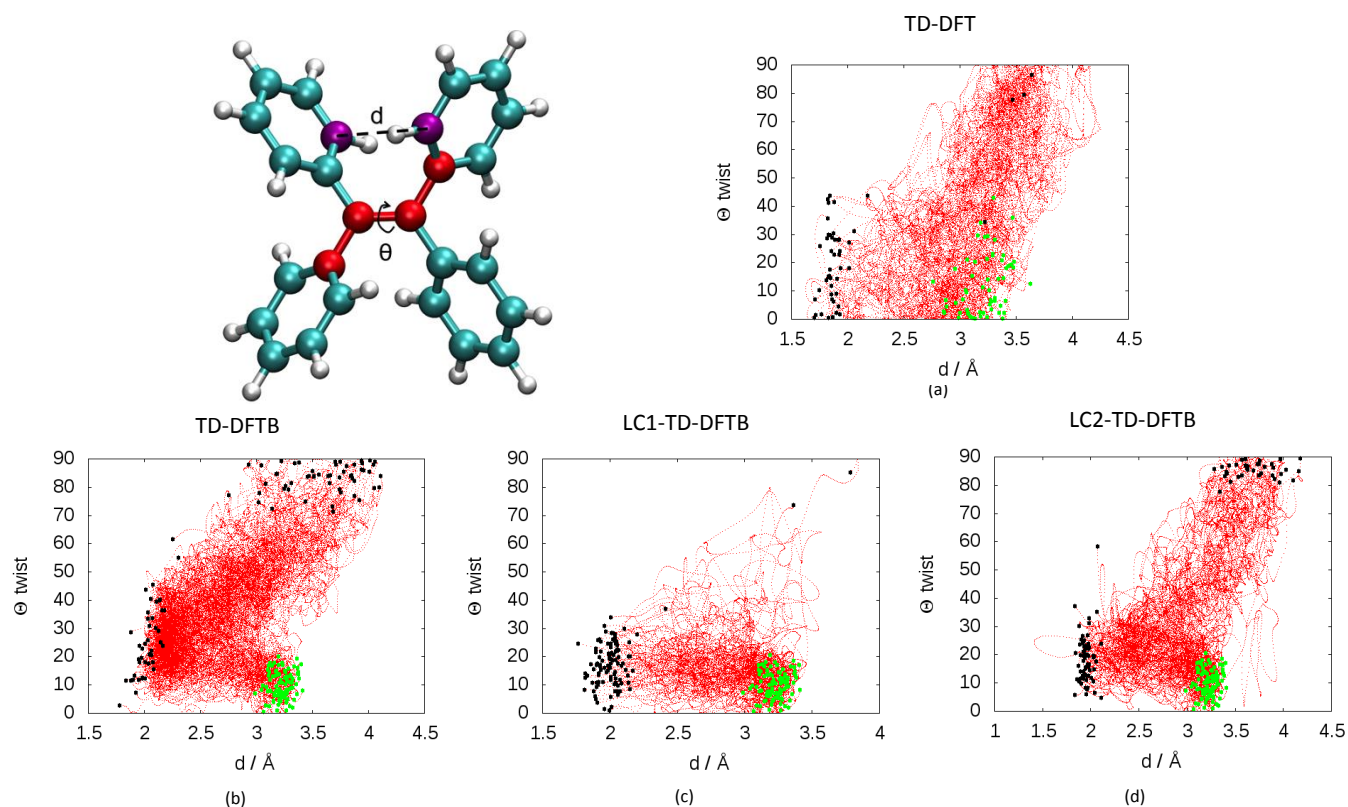


Fig. 3: Evolution of the distance d between the carbon atoms (in purple) involved in cyclization and the CC=CC (in red) dihedral angles θ of in the dynamics at: (a) TD-DFT (60 trajectories taken from previous work on TPE computed with PBE0/def2-SVP, see ref. 33) and 100 trajectories at (b) TD-DFTB, (c) LC1-TD-DFTB and (d) LC2-TD-DFTB levels. All dynamics were performed in the nonadiabatic regime except for standard TD-DFTB done within the adiabatic approximation. The C-C distance d corresponds to the minimum distance among the 8 possible C-C involved in cyclization at every step of the dynamics. The green dots represent the geometries of the initial condition for the different trajectories. The black dots represent the geometries corresponding to the S_1/S_0 crossing for the different trajectories.

electronic structure level employed. While LC1-TD-DFTB predicts that nonradiative decay almost entirely occurs via photocyclization, pure TD-DFTB (no long-range correction) clearly favors ethylenic twist pathway. TD-DFTB and LC1-TD-DFTB represent the two extrema for the ratio of deactivation mechanisms. While earlier theoretical work favored photocyclization, "pure" photocyclization as obtained with LC1 approach is inconsistent with recent experimental work that emphasize the important role of ethylenic twist.^{64,65} On the other hand, LC2-TD-DFTB predicts important role of both mechanisms, with the preference towards photocyclization. This is in line with our earlier TD-DFT nonadiabatic dynamics done with a hybrid functional (PBE0/def2-SVP).³³ This conclusion is further supported by the CASPT2 study of Thiel *et al* where the static profile of a TPE derivative shows photocyclization as a barrierless process whereas photoisomerization is less favorable due to the presence of a barrier (8.4 kcal/mol).³⁴ Nevertheless, among all available TD-DFTB approximations, LC2-TD-DFTB appears as the closest substitute of TD-DFT reference results.

In terms of vertical excitation energies (see Table S1 in ESI), pure TD-DFTB provides results similar to GGA functionals, *i.e.* underestimating excitation energies of the valence $\pi\pi^*$ states. Despite the TPE lowest lying singlet excited state not being a charge transfer state (see Table S2 and Fig. S1 in ESI), an improvement is observed upon usage of long-range correction for TD-DFTB. LC1 performs similarly to standard long-range corrected functionals with TD-DFT, upshifting the excitation energies. In contrast, LC2 method provides the results closer to standard hybrid functionals (such as B3LYP and PBE0), which is due to the different method employed for the implementation of long-range correction in LC2 approach.

Overall, the dynamic in the framework of LC2-TD-DFTB is able to qualitatively reproduce the result obtained at higher levels of theory. For that reason, the results presented in the main text are mainly based on LC2-TD-DFTB, while the full comparison of different methods is given in ESI.

3.1.2. TPE dynamics in solvent

To further validate the idea that the photocyclization is the main nonradiative deactivation pathway of TPE, adiabatic dynamics in the presence of hexane solvent is performed in the framework of LC2-TD-DFTB (see Fig. S9 and S10 in ESI), in order to interpret the experimental lifetimes. Among the 100 trajectories, 73 terminated close to the crossing point leading to cyclization and 27 terminated on a twisted state. Thus, the photocyclization can be observed in hexane and remains the major deactivation mechanism. The overall S_1 excited state lifetime is 0.8 ps. By separating two sets of trajectories corresponding to the two mechanisms, we obtained time constants of 0.3 ps and 2.2 ps for photocyclization and ethylenic twist, respectively.

Since cyclization appears as the dominant mechanism in all recent theoretical contributions, we try to reconcile theoretical predictions with the experiments. Greene³⁵ measured a transient absorption spectrum of TPE in hexane with a broad peak at 620 nm decaying on ultrafast timescale.

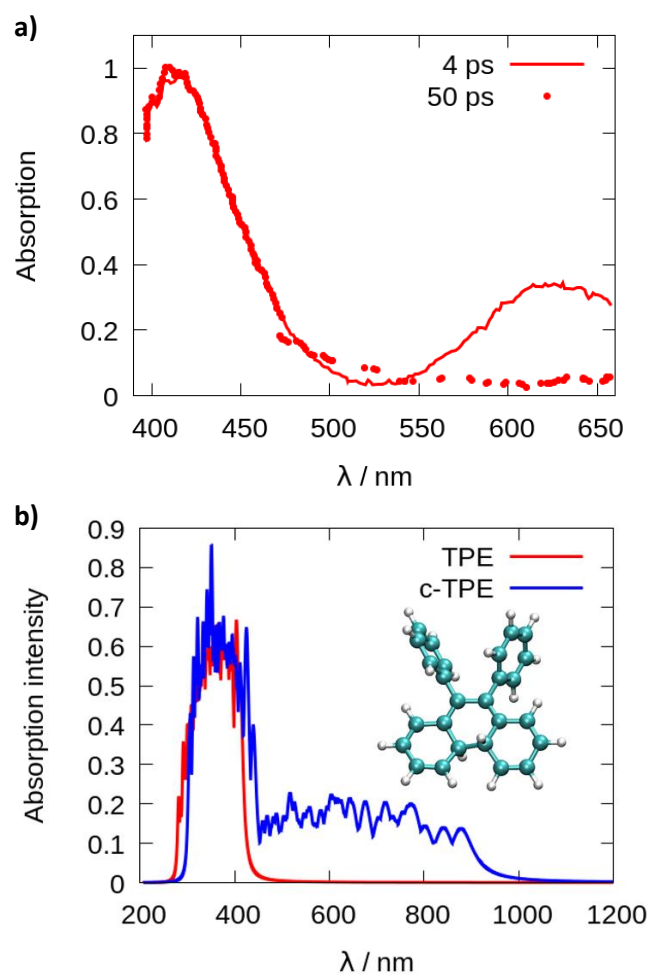


Fig. 4: Photoabsorption spectra (a) reproduced from the paper of Greene³⁴ and (b) computed from a Wigner distribution (ω B97XD/Def2-SVP) for TPE in red and the cyclized form of TPE (c-TPE) in blue, at LC2-TD-DFTB level for the isolated molecules.

The peak was explained in terms of excited state absorption. However, from the computed photoabsorption spectra (see Fig. 4), the broad peak centered around 600-650 nm observed by Greene could be attributed to the absorption of the cyclized form of TPE, biphenyl-dihydrophenanthrene (c-TPE). The disappearance of this peak within only several picoseconds, as observed by Greene, may be related to the degradation of c-TPE. However, c-TPE is expected to be stable following the Woodward-Hoffmann rules. Although beyond the present investigation, different hypotheses can explain the possible disappearance of c-TPE on ultrafast timescale: 1) Upon irradiation with visible light, the ring opening of c-TPE may occur through a conical intersection leading to TPE.³³ 2) The ring opening may occur in "hot" ground state: after relaxation through the conical intersection, the system has high excess energy which may help to overcome the barrier for cycloreversion before being dissipated to environment. 3) Upon formation of c-TPE, a side reaction may occur leading to the formation of side products which eventually convert to pristine TPE.⁷⁴ The rapid degradation of c-TPE could also explain why photocyclization was not recognized in most earlier experimental work on TPE. The existence of a photocyclized intermediate is still under debate even in recent

experimental work.^{65,66} In the spectroscopic results by Kayal *et al.*,⁶⁵ a bi-exponential decay of TPE was observed with a "short" time constant of 0.29 ps and a longer time constant of 1.9 ps in hexane. While the latter was assigned to ethylenic twist, the former was interpreted as a structural relaxation of the S_1 Franck-Condon state to a torsionally relaxed state.

In light of our current result, we were able to qualitatively reproduce the experimental lifetime of the twisted state. There is a major disagreement about the interpretation of the short time constant. **Experimentalists attribute this short time motion to the initial relaxation of excited state initiated by the torsion of the phenyl ring.**^{65,66} However, we note that the short time constant perfectly matches the photocyclization process observed in theoretical work. Another recent experimental work highlighted the existence of both deactivation mechanisms, demonstrating the limit of the RIM model to explain the AIE process in TPE and its derivatives.⁶⁶ However, the photocyclization was not considered as the main deactivation pathway for pristine TPE and the photocyclized intermediates were detected as long-lived species (for the derivatives of TPE). Thus, the further investigation should be done to correctly quantify the main deactivation pathways in TPE and reach the agreement between theory and experiment.

3.2 Excited state dynamics of DPDBF and DMTPS

The excited state decay of DPDBF and DMTPS in solution and aggregate was recently investigated by Blancafort *et al.*,^{19,20} computing the energy profiles at CASPT2. The results demonstrated the key role of conical intersections to rationalize the fluorescence quenching in solution. However, a static picture does not provide information about the excited state lifetime and may eventually lack information about the possible side mechanisms. Thus, our first goal is to compute the dynamics of these two model systems and to compare the observed deactivation mechanism to the results at CASPT2, in order to validate the accuracy of LC-TD-DFTB. The second aim is to investigate the effect of solvent on the nonradiative decay and the excited states lifetime.

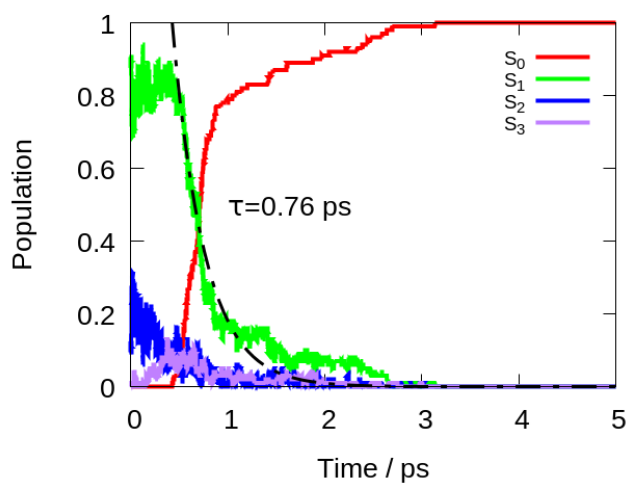


Fig. 5: Population of different electronic states of DPDBF in the gas phase with respect to time in the nonadiabatic dynamics at LC2-TD-DFTB. The exponential fitting for the decay of the population of excited states ($S_1 + S_2 + S_3$) is shown in black.

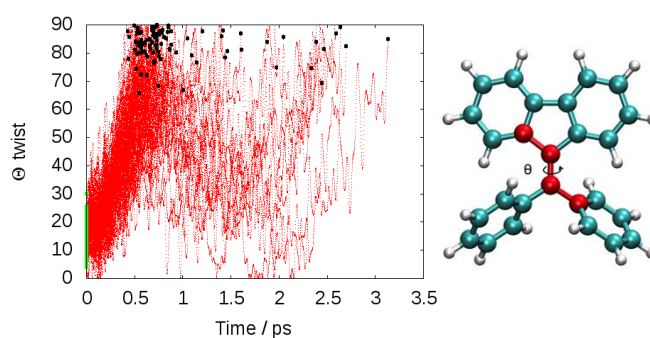


Fig. 6: Time evolution of the CC=CC dihedral angle Θ of DPDBF in gas phase for all 100 trajectories with dynamics at LC2-TD-DFTB. The black dots represent the geometries corresponding to the S_1/S_0 crossings, while the green dots (0 fs) represent the initial conditions.

In the Franck-Condon point, the excitation from S_0 to S_2 state of DPDBF at LC2-TD-DFTB corresponds to the bright $\pi\pi^*$ transition while S_1 has very small oscillatory strength (see Table S1 in ESI). By moving away from the Franck-Condon point, the S_2 state can re-cross the potential energy surface of S_1 and thus, the ordering of excited states may change. Following our protocol for sampling of initial conditions, part of the trajectories was initiated in the S_2 , and part in the S_1 , depending on which state carries more intensity.

The computed lifetime of the excited states populated in dynamics ($S_1 + S_2 + S_3$) for the isolated DPDBF is 0.8 ps (Fig. 5). To monitor the evolution of the different trajectories, the dihedral angle Θ for the twisting is plotted with respect to time (Fig. 6). The different trajectories reached the crossing point with a dihedral angle Θ close to 90° which corresponds to a twisted state. Thus, only a single mechanism is observed for the fluorescence quenching of DPDBF, which is the ethylenic twist. These results are consistent with the previous work of Blancafort *et al.*¹⁹ A nonadiabatic molecular dynamics study by Gao *et al.*³¹ which employed an approximate time dependent Kohn-Sham approach also provided similar results with respect to the deactivation mechanism.

The decay to the ground state through an ethylenic twist involves a large molecular motion and the presence of solvent

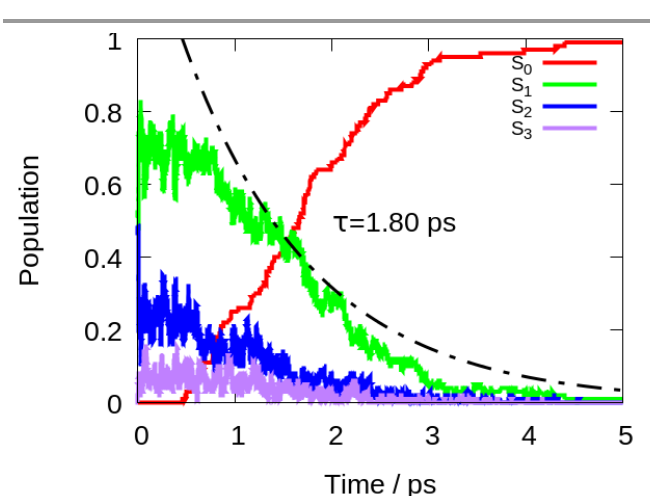


Fig. 7: Time evolution of the population of different electronic states of DMTPS in gas phase dynamic at LC2-TD-DFTB. The exponential fitting for the decay of the excited states ($S_1 + S_2 + S_3$) is shown in black.

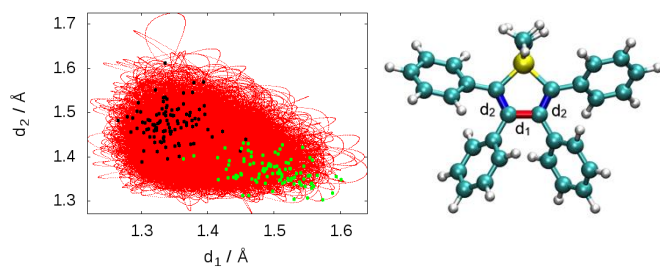


Fig. 8: Evolution of the bond length d_1 (red bond) and the average bond length d_2 (blue bonds) from dynamics at LC2-TD-DFTB. The black dots represent the geometry corresponding to the S_1/S_0 crossing for the different trajectories and the green dots corresponds to the geometries of initial conditions.

greatly increases the excited state lifetime compared to gas-phase. Excited state lifetime value of 8.15 ps was computed from nonadiabatic dynamic in hexane solvent (see Fig. S13 in ESI). 70% of the trajectories (21/30) proceed through an ethylenic twist characterized by large dihedral angle θ ($> 45^\circ$). This angle for DPDBF close to the S_1/S_0 crossing point is not as pronounced as in the gas-phase dynamics due to the more distorted geometries observed in the presence of hexane. Moreover, due to the steric effect by the surrounding solvent molecules, additional deactivation pathways appear for DPDBF such as photocyclization (1/30) and the distortion of benzene ring (3/30), which are not observed for the isolated molecule (note that 5 trajectories remain in excited state during the simulation time). All three mechanisms appear in both TPE and DPDBF, which can be rationalized by their similar conjugation pattern. DPDBF has a more rigid structure than TPE and thus, the photocyclization appear as a less favorable mechanism than the ethylenic twist. Further work with higher level of theory should be considered for DPDBF to validate the existence of these side mechanisms.

To describe the excited state dynamics of the DMTPS with LC2-TD-DFTB, a nonadiabatic simulation is necessary, since two lowest singlet excited states (S_1 and S_2) appear nearly degenerate at the Franck-Condon point. The computed gas phase excited state lifetime is 1.8 ps (Fig. 7). The evolution of C-C bond lengths in the silole ring (Fig. 8) shows an alternation of the three bond lengths near the crossing with the ground state (compared to the initial structures). The single bond d_1 shrinks from initial 1.4-1.6 Å to 1.25-1.45 Å while the average length of the double bond d_2 stretches from 1.3-1.4 Å to 1.4-1.6 Å.

The initial motion in the excited state dynamics is an in-plane vibration characterized by a bond length alternation of the single and double bonds of silole ring. The deactivation mechanism of DMTPS can be related to cyclopentadiene.⁷⁵ In cyclopentadiene derivatives, the conical intersection is reached by an in-plane motion conjugated with out-of-plane ring deformation. In DMTPS, the out-of-plane silicon can be observed for all the trajectories. Thus, the strong deplanarization facilitates reaching the S_1/S_0 crossing. Overall, the results (*i.e.* mechanisms) agree qualitatively with the previous computational work of Blancafort *et al.*²⁰

The presence of hexane solvent included *via* mechanical embedding does not change the deactivation mechanisms in

DMTPS (see Fig. S16 in ESI) compared to gas-phase dynamics. The computed excited state lifetime in hexane is 6 ps.

3.3 General discussions

The present results along with several previous computational works demonstrate the importance of conical intersections for the fluorescence quenching of the most representative AIE systems. Thus, the RACI model proposed by Blancafort *et al.* appears more suitable to explain the fluorescence quenching mechanism for these systems than the RIM model. While the two models can be reconciled by stating that RACI is just a more specific variant of RIM,²⁰ several remarks should be made. The RIM, *i.e.* its most common submodel RIR (restriction of intramolecular rotations) assumes a full rotation of the propeller-like moieties (such as phenyl rings). However, at the short timescales (*i.e.* femtosecond to picosecond) of the nonradiative decay, we do not observe rotations but rather limited torsions of rotatable groups. **The short time does not allow a full vibrational relaxation according to RIM model, whereas nonadiabatic events such as deactivation through a conical intersection are more likely to happen on such timescales.** Furthermore, the nonradiative deactivation does not comprise only photophysical, but also photochemical phenomena, such as cyclization. Likewise, the recent work of Tang *et al.* asserts that “the RIM paradigm needs to be revisited”.⁶⁶ The central role of conical intersections in fluorescence quenching of AIE systems should not be surprising considering that their importance was already recognized for many other organic molecules such as BODIPY,^{76,77} oxazine dye,⁷⁸ aminopurine,⁷⁹ polycyclic aromatic hydrocarbons⁸⁰ etc. The role of conical intersections was also discussed for AIE-active ES IPT (excited state intramolecular proton transfer) materials.^{81,82}

While the present work was done for the fundamental (*i.e.* pristine) AIE systems, most of the experimental work refers to the various derivatives of these molecules. The effect of the substituents cannot be neglected, as different functional groups can eventually completely change the accessible decay pathways.³⁴ Furthermore, the effect of solvent (polarity, viscosity) may be significant and should not be neglected when interpreting experimental results. For instance, changing solvent may significantly extend the lifetime of the excited state.³⁶ While the dynamics in hexane (low dielectric constant) strongly resembles the gas phase dynamics **with respect to deactivation mechanism**, this might not be universal for other solvents. These effects should be the focus of the future work.

4 Conclusions

We explore the mechanisms of the nonradiative decay in three prototypical AIE systems (TPE, DPDBF and DMTPS), both in the gas phase (reflecting the intrinsic molecular properties) and in hexane solution. The relaxation through the conical intersection plays a key role in the fluorescence quenching of these compounds. This goes in favor of the recently proposed RACI model, which exploits the concept of conical intersection accessibility to explain the fluorescence quenching in solution.

TPE (both intrinsic and solvated) has two major excited state deactivation channels: photocyclization and ethylenic twist. DPDBF mainly decays through the ethylenic twist, while DMTPS decays via silole ring distortion. The hexane solvent does not significantly alter the photophysics and photochemistry of these compounds. The mechanisms which involve a sizable geometrical reorganization (ethylenic twist) and ring distortion occur on a longer timescale, while the photocyclization is only slightly slower in solution. The computational protocol we employ here, combining excited state molecular dynamics and cheap electronic structure method (LC-TD-DFTB) provides a reliable picture of excited state phenomena at the previously unprecedented computational speed. Thus, the same methodology will be further employed for rational design and screening of new AIE molecules.

TD-DFTB is an emerging and promising method for investigating the excited state phenomena in large molecules. Earlier applications by Mitric *et al.* and Barbatti *et al.* outlined the strengths and weaknesses of this approach.^{83,84} Common AIE systems appear suitable for LC-TD-DFTB, since their photochemistry and photophysics are restricted to low-lying excited states (typically S_1 , S_2) of $\pi\pi^*$ character. The present results are consistent with the earlier theoretical and available experimental data. In the cases where consensus is still not achieved, such as photocyclization of TPE, LC-TD-DFTB results still qualitatively agree with other theoretical methods (TD-DFT, CASPT2, semi-empirical). Yet, the precise quantitative measures (lifetimes, ratios) are still highly sensitive to the approximation employed (both for nuclear dynamics and electronic structure) and should serve only as a qualitative guideline to interpret experiments.

Conflicts of interest

There are no conflicts to declare.

Acknowledgements

EPFL is acknowledged for funding support.

Notes and references

- 1 K. Kikuchi, *Chem. Soc. Rev.*, 2010, **39**, 2048–2053.
- 2 N. Boens, V. Leen and W. Dehaen, *Chem. Soc. Rev.*, 2012, **41**, 1130–1172.
- 3 L. Yuan, W. Lin, K. Zheng and S. Zhu, *Acc. Chem. Res.*, 2013, **46**, 1462–1473.
- 4 S. Kolemen, O. A. Bozdemir, Y. Cakmak, G. Barin, S. Erten-Ela, M. Marszalek, J.-H. Yum, S. M. Zakeeruddin, M. K. Nazeeruddin, M. Grätzel and E. U. Akkaya, *Chem. Sci.*, 2011, **2**, 949–954.
- 5 Y. Ge and D. F. O'Shea, *Chem. Soc. Rev.*, 2016, **45**, 3846–3864.
- 6 B. Gu, W. Wu, G. Xu, G. Feng, F. Yin, P. H. J. Chong, J. Qu, K. T. Yong and B. Liu, *Adv. Mater.*, 2017, **29**, 1701076.
- 7 J. Luo, Z. Xie, J. W. Y. Lam, L. Cheng, B. Z. Tang, H. Chen, C. Qiu, H. S. Kwok, X. Zhan, Y. Liu and D. Zhu, *Chem. Commun.*, 2001, **381**, 1740–1741.
- 8 J. Mei, N. L. C. Leung, R. T. K. Kwok, J. W. Y. Lam and B. Z. Tang, *Chem. Rev.*, 2015, **115**, 11718–11940.
- 9 Y. Hong, J. W. Y. Lam and B. Z. Tang, *Chem. Soc. Rev.*, 2011, **40**, 5361–5388.
- 10 Y. Hong, *Methods Appl. Fluoresc.*, 2016, **4**, 022003.
- 11 S. Chen, H. Wang, Y. Hong and B. Z. Tang, *Mater. Horiz.*, 2016, **3**, 283–293.
- 12 R. T. K. Kwok, C. W. T. Leung, J. W. Y. Lam and B. Z. Tang, *Chem. Soc. Rev.*, 2015, **44**, 4228–4238.
- 13 M. Gao and B. Z. Tang, *ACS Sensors*, 2017, **2**, 1382–1399.
- 14 D. Volyniuk, J. Sutaite, A. Tomkeviciene, N. Kostiv, G. Buika and J. V. Grazulevicius, *J. Lumin.*, 2017, **192**, 534–540.
- 15 Y. Hong, J. W. Y. Lam and B. Z. Tang, *Chem. Commun.*, 2009, 4332–4353.
- 16 Q. Zeng, Z. Li, Y. Dong, C. Di, A. Qin, Y. Hong, L. Ji, Z. Zhu, C. K. W. Jim, G. Yu, Q. Li, Z. Li, Y. Liu, J. Qin and B. Z. Tang, *Chem. Commun.*, 2007, **1**, 70–72.
- 17 T. Nishiuchi, K. Tanaka, Y. Kuwatani, J. Sung, T. Nishinaga, D. Kim and M. Iyoda, *Chem. Eur. J.*, 2013, **19**, 4110–4116.
- 18 N. L. C. Leung, N. Xie, W. Yuan, Y. Liu, Q. Wu, Q. Peng, Q. Miao, J. W. Y. Lam and B. Z. Tang, *Chem. Eur. J.*, 2014, **20**, 15349–15353.
- 19 Q. Li and L. Blancafort, *Chem. Commun.*, 2013, **49**, 5966–5968.
- 20 X.-L. Peng, S. Ruiz-Barragan, Z.-S. Li, Q.-S. Li and L. Blancafort, *J. Mater. Chem. C*, 2016, **4**, 2802–2810.
- 21 L. Blancafort, R. Crespo-Otero and Q. Li, *Chem. Asian J.*, 2018, asia.201801649.
- 22 Y. Liu, X. Tao, F. Wang, J. Shi, J. Sun, W. Yu, Y. Ren, D. Zou and M. Jiang, *J. Phys. Chem. C*, 2007, **111**, 6544–6549.
- 23 B. K. An, S. K. Kwon, S. D. Jung and S. Y. Park, *J. Am. Chem. Soc.*, 2002, **124**, 14410–14415.
- 24 B. K. An, D. S. Lee, J. S. Lee, Y. S. Park, H. S. Song and S. Y. Park, *J. Am. Chem. Soc.*, 2004, **126**, 10232–10233.
- 25 Y. Sonoda, S. Tsuzuki, M. Goto, N. Tohnai and M. Yoshida, *J. Phys. Chem. A*, 2010, **114**, 172–182.
- 26 H. Wang, E. Zhao, J. W. Y. Lam and B. Z. Tang, *Mater. Today*, 2015, **18**, 365–377.
- 27 J. Shi, N. Chang, C. Li, J. Mei, C. Deng, X. Luo, Z. Liu, Z. Bo, Y. Q. Dong and B. Z. Tang, *Chem. Commun.*, 2012, **48**, 10675–10677.
- 28 E. P. J. Parrott, N. Y. Tan, R. Hu, J. A. Zeitler, B. Z. Tang and E. Pickwell-MacPherson, *Mater. Horiz.*, 2014, **1**, 251–258.
- 29 G.-J. Zhao, K.-L. Han, Y.-B. Lei and Y.-S. Dou, *J. Chem. Phys.*, 2007, **127**, 94307.
- 30 M.-C. Li, M. Hayashi and S.-H. Lin, *J. Phys. Chem. A*, 2011, **115**, 14531–14538.
- 31 X. Gao, Q. Peng, Y. Niu, D. Wang and Z. Shuai, *Phys. Chem. Chem. Phys.*, 2012, **14**, 14207–14216.
- 32 Z. Zhao, B. He and B. Z. Tang, *Chem. Sci.*, 2015, **6**, 5347–5365.
- 33 A. Prlj, N. Došlić and C. Corminboeuf, *Phys. Chem. Chem. Phys.*, 2016, **18**, 11606–11609.
- 34 Y. J. Gao, X. P. Chang, X. Y. Liu, Q. S. Li, G. Cui and W. Thiel,

- J. Phys. Chem. A*, 2017, **121**, 2572–2579.
- 35 B. I. Greene, *Chem. Phys. Lett.*, 1981, **79**, 51–53.
- 36 P. F. Barbara, S. D. Rand and P. M. Rentzepis, *J. Am. Chem. Soc.*, 1981, **103**, 2156–2162.
- 37 E. Lenderink, K. Duppen and D. A. Wiersma, *J. Phys. Chem.*, 1995, **99**, 8972–8977.
- 38 M. A. Robb, M. Garavelli, M. Olivucci and F. Bernardi, in *Reviews in Computational Chemistry*, John Wiley & Sons, Inc., 2007, pp. 87–146.
- 39 T. Frauenheim, G. Seifert, M. Elstner, T. Nienhaus, C. Köhler, M. Amkreutz, M. Sternberg, Z. Hajnal, A. Di Carlo and S. Suhai, *J. Phys. Condens. Matter*, 2002, **14**, 3015–3047.
- 40 A. Domínguez, B. Aradi, T. Frauenheim, V. Lutsker and T. A. Niehaus, *J. Chem. Theory Comput.*, 2013, **9**, 4901–4914.
- 41 A. Humeniuk and R. Mitrić, *J. Chem. Phys.*, 2015, **143**, 134120.
- 42 A. Humeniuk and R. Mitrić, *Comput. Phys. Commun.*, 2017, **221**, 174–202.
- 43 E. Titov, A. Humeniuk and R. Mitric, *Phys. Chem. Chem. Phys.*, 2018, **20**, 25995–26007.
- 44 V. Lutsker, B. Aradi and T. A. Niehaus, *J. Chem. Phys.*, 2015, **143**, 184107.
- 45 J. J. Kranz, M. Elstner, B. Aradi, T. Frauenheim, V. Lutsker, A. D. Garcia and T. A. Niehaus, *J. Chem. Theory Comput.*, 2017, **13**, 1737–1747.
- 46 J.-D. Chai and M. Head-Gordon, *Phys. Chem. Chem. Phys.*, 2008, **10**, 6615–6620.
- 47 F. Weigend, *Phys. Chem. Chem. Phys.*, 2006, **8**, 1057–1065.
- 48 M. J. Frisch, G. W. Trucks, H. B. Schlegel, G. E. Scuseria, M. A. Robb, J. R. Cheeseman, G. Scalmani, V. Barone, B. Mennucci, G. A. Petersson, H. Nakatsuji, M. Caricato, X. Li, H. P. Hratchian, A. F. Izmaylov, J. Bloino, G. Zheng, J. L. Sonnenberg, M. Hada, M. Ehara, K. Toyota, R. Fukuda, J. Hasegawa, M. Ishida, T. Nakajima, Y. Honda, O. Kitao, H. Nakai, T. Vreven, J. A. Montgomery, J. E. Peralta, F. Ogliaro, M. Bearpark, J. J. Heyd, E. Brothers, K. N. Kudin, V. N. Staroverov, R. Kobayashi, J. Normand, K. Raghavachari, A. Rendell, J. C. Burant, S. S. Iyengar, J. Tomasi, M. Cossi, N. Rega, J. M. Millam, M. Klene, J. E. Knox, J. B. Cross, V. Bakken, C. Adamo, J. Jaramillo, R. Gomperts, R. E. Stratmann, O. Yazyev, A. J. Austin, R. Cammi, C. Pomelli, J. W. Ochterski, R. L. Martin, K. Morokuma, V. G. Zakrzewski, G. A. Voth, P. Salvador, J. J. Dannenberg, S. Dapprich, A. D. Daniels, Farkas, J. B. Foresman, J. V. Ortiz, J. Cioslowski and D. J. Fox, *Gaussian 09, Revis. D.01, Gaussian, Inc., Wallingford CT*, 2009.
- 49 F. Furche, R. Ahlrichs, C. Hättig, W. Klopper, M. Sierka and F. Weigend, *Wiley Interdiscip. Rev. Comput. Mol. Sci.*, **4**, 91–100.
- 50 B. Aradi, B. Hourahine and T. Frauenheim, *J. Phys. Chem. A*, 2007, **111**, 5678–5684.
- 51 S. Pronk, S. Páll, R. Schulz, P. Larsson, P. Bjelkmar, R. Apostolov, M. R. Shirts, J. C. Smith, P. M. Kasson, D. Van Der Spoel, B. Hess and E. Lindahl, *Bioinformatics*, 2013, **29**, 845–854.
- 52 M. J. Abraham, T. Murtola, R. Schulz, S. Páll, J. C. Smith, B. Hess and E. Lindahl, *SoftwareX*, 2015, **1–2**, 19–25.
- 53 J. M. Wang, R. M. Wolf, J. W. Caldwell, P. A. Kollman and D. A. Case, *J. Comput. Chem.*, 2004, **25**, 1157–1174.
- 54 J. C. Tully, *J. Chem. Phys.*, 1990, **93**, 1061.
- 55 D. Hollas, J. Suchan, M. Oncak and P. Slavicek, P. ABIN, ZENODO, 2018, DOI: 10.5281/zenodo.1228462.
- 56 M. Ruckebauer, M. Barbatti, T. Müller and H. Lischka, *J. Phys. Chem. A*, 2010, **114**, 6757–6765.
- 57 L. Martinez, R. Andrade, E. G. Birgin and J. M. Martinez, *J. Comput. Chem.*, 2009, **30**, 2157–2164.
- 58 G. Bussi, D. Donadio and M. Parrinello, *J. Chem. Phys.*, 2007, **126**, 14101.
- 59 F. Plasser, R. Crespo-Otero, M. Pederzoli, J. Pittner, H. Lischka and M. Barbatti, *J. Chem. Theory Comput.*, 2014, **10**, 1395–1405.
- 60 M. Barbatti and R. Crespo-Otero, in *Density-Functional Methods for Excited States*, eds. N. Ferré, M. Filatov and M. Huix-Rotllant, Springer International Publishing, Cham, 2016, pp. 415–444.
- 61 J. Ma, M. B. Zimmt, G. B. Dutt and D. H. Waldeck, *J. Am. Chem. Soc.*, 1994, **116**, 10619–10629.
- 62 N. B. Shustova, T. C. Ong, A. F. Cozzolino, V. K. Michaelis, R. G. Griffin and M. Dincă, *J. Am. Chem. Soc.*, 2012, **134**, 15061–15070.
- 63 Z. Yang, W. Qin, N. L. C. Leung, M. Arseneault, J. W. Y. Lam, G. Liang, H. H. Y. Sung, I. D. Williams and B. Z. Tang, *J. Mater. Chem. C*, 2016, **4**, 99–107.
- 64 K. Kokado, T. Machida, T. Iwasa, T. Taketsugu and K. Sada, *J. Phys. Chem. C*, 2018, **122**, 245–251.
- 65 S. Kayal, K. Roy, S. Umaphathy, S. Kayal, K. Roy and S. Umaphathy, *J. Chem. Phys.*, 2018, **148**, 024301.
- 66 Y. Cai, L. Du, K. Samedov, X. Gu, F. Qi, H. H. Y. Sung, B. O. Patrick, Z. Yan, X. Jiang, H. Zhang, J. W. Y. Lam, I. D. Williams, D. Lee Phillips, A. Qin and B. Z. Tang, *Chem. Sci.*, 2018, **9**, 4662–4670.
- 67 N.-W. Tseng, J. Liu, J. C. Y. Ng, J. W. Y. Lam, H. H. Y. Sung, I. D. Williams and B. Z. Tang, *Chem. Sci.*, 2012, **3**, 493–497.
- 68 H. H. Klingenberg, E. Lippert and W. Rapp, *Chem. Phys. Lett.*, 1973, **18**, 417–419.
- 69 D. A. Shultz and M. A. Fox, *J. Am. Chem. Soc.*, 1989, **111**, 6311–6320.
- 70 F. B. Mallory, C. S. Wood and J. T. Gordon, *J. Am. Chem. Soc.*, 1964, **86**, 3094–3102.
- 71 R. J. Olsen and R. E. Buckles, *J. Photochem.*, 1979, **10**, 215–220.
- 72 M. P. Aldred, C. Li and M. Q. Zhu, *Chem. Eur. J.*, 2012, **18**, 16037–16045.
- 73 G. Huang, B. Ma, J. Chen, Q. Peng, G. Zhang, Q. Fan and D. Zhang, *Chem. Eur. J.*, 2012, **18**, 3886–3892.
- 74 A. Jain, A. Achari, N. Mothi, M. Eswaramoorthy and S. J. George, *Chem. Sci.*, 2015, **6**, 6334–6340.
- 75 T. S. Kuhlman, W. J. Glover, T. Mori, K. B. Møller and T. J. Martínez, *Faraday Discuss.*, 2012, **157**, 193–212.
- 76 A. Prlj, A. Fabrizio and C. Corminboeuf, *Phys. Chem. Chem. Phys.*, 2016, **18**, 32668–32672.
- 77 A. Prlj, L. Vannay and C. Corminboeuf, *Helv. Chim. Acta*, 2017, **100**, e1700093.

- 78 J. Brazard, L. A. Bizimana, T. Gellen, W. P. Carbery and D. B. Turner, *J. Phys. Chem. Lett.*, 2016, **7**, 14–19.
- 79 M. Barbatti and H. Lischka, *Phys. Chem. Chem. Phys.*, 2015, **17**, 15452–15459.
- 80 Y. Harabuchi, T. Taketsugu and S. Maeda, *Phys. Chem. Chem. Phys.*, 2015, **17**, 22561–22565.
- 81 M. Dommett, M. Rivera and R. Crespo-Otero, *J. Phys. Chem. Lett.*, 2017, **8**, 6148–6153.
- 82 M. Dommett and R. Crespo-Otero, *Phys. Chem. Chem. Phys.*, 2017, **19**, 2409–2416.
- 83 J. Hoche, H.-C. Schmitt, A. Humeniuk, I. Fischer, R. Mitrić and M. I. S. Röhr, *Phys. Chem. Chem. Phys.*, 2017, **19**, 25002–25015.
- 84 L. Stojanović, S. G. Aziz, R. H. Hilal, F. Plasser, T. A. Niehaus and M. Barbatti, *J. Chem. Theory Comput.*, 2017, **13**, 5846–5860.